



Aircraft Stability Characteristics in a Single Horizontal Tail Failure and Evaluation of Countermeasures for Safe Landing

I. Arif ^{1†}, T. Q. Ansari ¹ and A. Javed ²

¹ Department of Mechanical Engineering, The Hong Kong Polytechnic University, Hung Hom, Kowloon, Hong Kong

² Department of Aerospace Engineering, College of Aeronautical Engineering, National University of Sciences & Technology, Islamabad, Pakistan

†Corresponding Author Email: arsalan_sayani@cae.nust.edu.pk

(Received July 1, 2020; accepted October 28, 2020)

ABSTRACT

This paper presents the stability characteristics of a high-speed aircraft in a possible emergency situation of a single horizontal tail failure during flight. The flight control system of the aircraft under study operates with a fail-safe mechanism where the malfunctioned horizontal tail is self-locked in neutral position, while the other tail can normally perform its operations. However, in such a scenario the aircraft is required to land at the nearest airfield on priority. Computational analysis is carried out to analyze the stability characteristics of the aircraft under this emergency where it is subjected to adverse pitching, rolling and yawing moments due to the locked horizontal tail. For computational analysis, a unique analysis technique is employed to isolate the horizontal tail geometry from aircraft and domain which helps in geometry/mesh consistency, even with different horizontal tail deflections. The results of baseline configuration are validated with literature and subsequently, the analysis is carried out at various flow conditions, horizontal tail deflections and ground clearances. A complete flight envelope is determined based on horizontal tail, ailerons and rudder deflection along with landing angle of attack for safe landing. The study can help in further improvement of the aircraft flight control computer to restrict the tail, aileron and rudder deflections up to the evaluated safe limits. Also, the designed methodology is applicable to all similar aircraft.

Keywords: Control surfaces; Flight envelope; Landing; Performance; Stability and control.

NOMENCLATURE

AoA	angle of attack	m	meter
C_D	coefficient of drag	OEM	original equipment manufacturer
C_L	coefficient of lift	SA	Spalart-Allmaras turbulence model
C_l	coefficient of rolling moment	RANS	Reynolds Averaged Navier Stokes equations
C_m	coefficient of pitching moment	y+	Non-dimensional length scale associated with turbulence model
C_n	coefficient of yawing moment		
CG	centre of gravity		
FCS	flight control system		
HT	Horizontal Tail	δ_a	aileron deflection
M	Mach number	δ_r	rudder deflection
MFR	Mass Flow Rate		

1. INTRODUCTION

Flight dynamics of aircraft including stability and control characterizes the aircraft response to

dynamic perturbations and control inputs. It is one of the most critical features for a high-speed aircraft which are designed to have high maneuverability as well as advanced control mechanism (Cook 2012). Modern day aircraft are equipped with advanced

Flight Control System (FCS) which includes mechanical control and redundant digital control system (Raymer 2012). These systems are well programmed to maintain the aircraft stability during different flight operations, however, during certain control surface failures, the aircraft is subjected to adverse forces and moments where manual control is required and hence a comprehensive knowledge regarding the aircraft stability characteristics is required to control and safely land the aircraft. Stability analysis of an aircraft at low angle of attack (AoA) has received significant importance over the years where the dynamic behavior of aircraft can be accurately predicted by analytical methods due to low/mild variations in stability derivatives. However, the determination of stability characteristics becomes substantially complex for high-speed aircraft at relatively high AoA such as modern military aircraft. This phenomenon is attributed to the fact that the stability behavior at high AoA involves various non-linearities such as modes coupling, and frequency effects, and therefore cannot be analyzed by simple linear analytical methods (Cook 2012). Orlik-Rückemann (1975) identified the requirement of non-linear methods for determination of aircraft stability at high AoA. He observed that the unsteady motion of aircraft at high AoAs modifies the aerodynamic forces acting on it and affects its dynamic behavior as well. Hence, the aircraft stability characteristics can only be analyzed by solving the unsteady flow equations and equations of motion of body simultaneously at each instance. This approach can predict the aircraft stability and control characteristics, however, it is deemed impractical due to high complexity in mathematical formulations (Chyu and Schiff 1983). A simplified method was later proposed where the flow equations were decoupled from inertial equations and were subsequently linearized to determine the dynamic response (Hui and Tobak 1984).

There exist four common methods to determine the stability characteristics of an aircraft. These include flight test method (Kimberlin 2003), wind tunnel test (Neal *et al.* 2004), analytical modeling (Stevens *et al.* 2015; Hua *et al.* 2017; Zhiqun and Pinqi 2017) and computational methods (Murman *et al.* 2002; Rogers *et al.* 2003). Although, actual flight test of aircraft is one of the most accurate methods (Kimberlin 2003), however these tests involve high testing costs, large human resource and above all, it requires a real aircraft which might not be available at the early design phase of aircraft. Furthermore, it may also jeopardize the safety of aircraft as well due to testing at the early design phase. A common method to determine aircraft stability and control is wind tunnel testing (Neal *et al.* 2004; Jing *et al.* 2016). Wind tunnel testing also requires certain physical resources and the analysis is subjected to certain limitations such as blockage effects, model scaling, and flow interference etc. Another method of stability analysis involves analytical and theoretical modelling and data extraction (Stevens *et al.* 2015; Zhiqun and Pinqi 2017). The method is simple in its application and can accurately predict the flight performance of aircraft at moderate conditions, however, the accuracy is adversely hampered at high AoA

conditions due to associated non-linearities. In the last few decades, with the advancement in numerical modeling techniques and computational resources, computational fluid dynamics (CFD) has emerged as a powerful tool to determine the stability and control characteristics of an aircraft. The method has been widely used in recent times due to advancements in computational resources. Numerical analysis have been successfully carried out to evaluate stability and control for vehicle design (Murman *et al.* 2002; Rogers *et al.* 2003) which signifies its feasibility in complex problems. Also, an automatic differentiation to potential flow solver using CFD code was successfully applied to predict stability and control derivatives (Park *et al.* 1999; Green *et al.* 2004). An in-flight stability analysis of X-48B aircraft was also carried out using numerical analysis (Regan 2008).

Evaluation of stability characteristics in an asymmetric condition with the control surface locked at a particular position with different flight conditions involves severe complexities and requires detailed information regarding aircraft attitude and parameters at each instance to determine the aircraft stability derivatives. Hence, it becomes practically impossible to evaluate the stability characteristics of aircraft under these circumstances using available theoretical models. Furthermore, the available data in literature does not highlight the aircraft response in particular emergency situations. Hence, the aircraft stability characteristics during different flight conditions can be analyzed by numerical methods and control actions can be proposed. In this study, we aim to ascertain aerodynamic and stability characteristics of the aircraft with left horizontal tail (HT) failure and evaluate the proposed landing limits using other functional control surfaces including right HT, ailerons and rudder. The aircraft in this situation would be subjected to adverse moments due to asymmetric HT movements, hence, the determination of aircraft behavior and response becomes quite complex. Since the flight manuals and literature does not present any possible solutions, this research would provide a baseline analysis for such emergency situations encountered by any high-speed aircraft. Furthermore, the analysis can help in further improvement of the flight control system to restrict the aircraft tail, aileron and rudder deflections up to the evaluated safe limits.

This paper is organized as follows. An overview of flight control system of the aircraft is presented in Section 2. Then in Section 3, details of computational setup and numerical modeling are presented. A brief on validation of numerical scheme with literature and Wind Tunnel Data is also presented in this section. Subsequently, aircraft aerodynamic and stability characteristics based on HT deflections and different ground clearances are discussed in Section 4 which is followed by evaluation of countermeasures for safe landing.

2. OVERVIEW OF FLIGHT CONTROL SYSTEM

The Flight Control System (FCS) of aircraft under

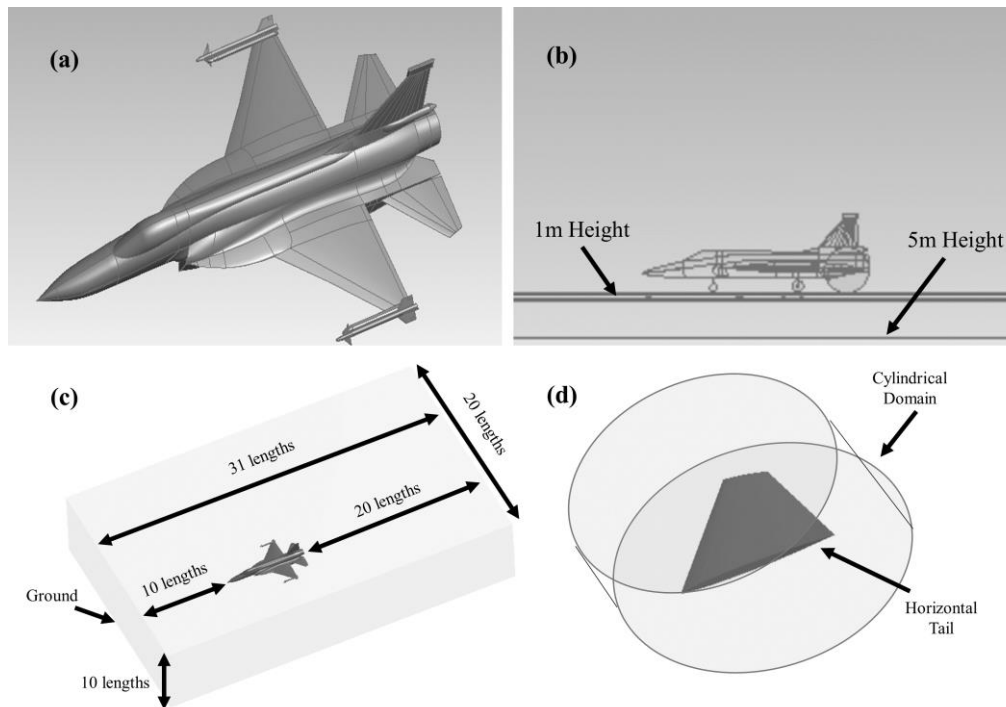


Fig. 1. (a) CAD model of aircraft, (b) Interfacing of different ground clearances with aircraft domain, (c) computational domain (scale not to size) and (d) horizontal tail in a cylindrical domain.

study has a full-authority quadruple redundant digital system with dual-redundancy in the pitch axis, and mechanical control plus dual-redundant digital control augmentation in roll and yaw axes. The main control surfaces are ailerons, HTs and rudder. Auxiliary control surfaces are leading-edge flaps, speed brakes, and trailing-edge flaps. FCS amplifies pilot input, air data information and aircraft motion sensor signals. After computation of redundancy and control law, it provides required control commands for the hydraulic servo actuators that control the HTs, the lateral electric servo actuators that control ailerons and the directional electric servo actuator that controls the rudder. In case of any mechanical, electrical or hydraulic failure of a HT, the FCS automatically locks the malfunctioned tail into neutral position at zero incidence angle. The functional HT can be controlled normally, however, the aircraft experiences degradation in its performance and stability characteristics. In this particular emergency, the aircraft is required to be landed on priority. The aerodynamic characteristics of the aircraft are bound to change when the aircraft is in close proximity of the ground during landing and take-off. The ground-effect starts to affect aircraft stability when it is within half-span close to the ground. The swirling of air and the wingtip vortices are the two major causes of drag on the aircraft. Hence, this research aims to investigate the aerodynamic behavior of aircraft under the HT locked emergency and analyze the safe landing limits using functional control surfaces of the aircraft.

3. COMPUTATIONAL SETUP AND NUMERICAL MODELLING

3.1 Geometry and Modelling

For numerical analysis involving complex geometries such as an aircraft, geometry modeling is one of the most challenging tasks. A verified CAD model of the aircraft is utilized for the current study (Masud *et al.* 2015; Masud *et al.* 2017). The additional features such as external stores, gun and wing attachments except wingtip missiles are removed from the model for simplicity. Since the emergency situation requires the aircraft to land immediately which involves the operations of landing gears, the landing gears are modeled by measuring the exact dimensions of the component assembly on aircraft. Furthermore, the HTs are detached from the aircraft assembly to facilitate its rotations at different incidence angles for the analysis without affecting the aircraft geometry/mesh. Fig. 1(a) shows the complete assembled aircraft model which is utilized for numerical analysis. A rectangular domain is generated around the aircraft geometry and its size is set 20 times the aircraft length in downstream direction and 10 times the aircraft length in upstream direction to accurately model flight conditions away and in the near vicinity of aircraft without the influence of far field (Masud and Akram 2011). Since the analysis involves asymmetric deflections and the influence of side forces at different instances, the symmetry condition could not be applied. Hence, the domain is extended to 10 times the aircraft length in the spanwise

direction from both wings. A schematic of computational domain is shown in Fig. 1(c). The ground is modeled with careful considerations at two different heights with respect to aircraft during landing, i.e. 1m and 5m to evaluate the aircraft stability characteristics and control surface effectiveness during different conditions as shown in Fig. 1(b).

3.2 Solution Strategy

For numerical analysis, the accuracy of results greatly depends on the mesh structure and quality. Since the present study requires analysis at different ground heights with multiple HT deflections, it is imperative to maintain the mesh consistency for all simulation cases. Hence, we employed a unique solution strategy of geometric assembling/append approach where the HTs are embedded in separate cylindrical domains and appended with aircraft to maintain the mesh consistency as shown in Fig. 1(d). This feature helps in simulating the HTs at different incidence angles by just rotating the HT (within the circular domain) without affecting the aircraft geometry and thus maintaining the mesh consistency at all flow conditions. A similar approach is employed for modeling ground surface as well where different ground heights (1m and 5m) are appended with primary aircraft domain to analyze the characteristics of aircraft at these conditions without affecting the mesh consistency (as shown in Fig. 1(c)). Though the employed scheme is complex in its implementation due to presence of multiple sub-domains and requires prior planning in domain modeling/interfaces, it serves two major purposes. Firstly, the numerical solution of clean aircraft model excluding HTs can be simulated until the flow variables are stabilized. Subsequently, HTs are appended and the solution is progressed at different incidence angles which saves computational time/cost by 60%. Secondly, the mesh consistency remains unaffected at all HT deflections to ensure high accuracy in numerical solutions.

3.3 Numerical Approach

The numerical approach employed in the current study is similar to the research carried out by Masud *et al.* (Masud *et al.* 2017), which is also utilized in validation for baseline analysis of aircraft under normal flight conditions (without the HT failure). In order to analyze the flow characteristics and its dynamics in complex turbulent flow, the set of N-S equations consisting of continuity, momentum and energy are solved. The governing conservation equations are;

Conservation of Mass:

$$-\frac{\partial \rho}{\partial t} = \frac{\partial(\rho u)}{\partial x} + \frac{\partial(\rho v)}{\partial y} + \frac{\partial(\rho w)}{\partial z} \quad (1)$$

Conservation of Momentum:

$$\rho \left(\frac{\partial u}{\partial t} + u \frac{\partial u}{\partial x} + v \frac{\partial u}{\partial y} + w \frac{\partial u}{\partial z} \right) = -\frac{\partial p}{\partial x} + \mu \left(\frac{\partial^2 u}{\partial x^2} + \frac{\partial^2 u}{\partial y^2} + \frac{\partial^2 u}{\partial z^2} \right) + F_x \quad (2)$$

$$\rho \left(\frac{\partial v}{\partial t} + u \frac{\partial v}{\partial x} + v \frac{\partial v}{\partial y} + w \frac{\partial v}{\partial z} \right) = -\frac{\partial p}{\partial y} + \mu \left(\frac{\partial^2 v}{\partial x^2} + \frac{\partial^2 v}{\partial y^2} + \frac{\partial^2 v}{\partial z^2} \right) + F_y \quad (3)$$

$$\rho \left(\frac{\partial w}{\partial t} + u \frac{\partial w}{\partial x} + v \frac{\partial w}{\partial y} + w \frac{\partial w}{\partial z} \right) = -\frac{\partial p}{\partial z} + \mu \left(\frac{\partial^2 w}{\partial x^2} + \frac{\partial^2 w}{\partial y^2} + \frac{\partial^2 w}{\partial z^2} \right) + F_z \quad (4)$$

Conservation of Energy:

$$\rho C_p \left(\frac{\partial T}{\partial t} + u \frac{\partial T}{\partial x} + v \frac{\partial T}{\partial y} + w \frac{\partial T}{\partial z} \right) = \Phi + \frac{\partial}{\partial x} \left[k \frac{\partial T}{\partial x} \right] + \frac{\partial}{\partial y} \left[k \frac{\partial T}{\partial y} \right] + \frac{\partial}{\partial z} \left[k \frac{\partial T}{\partial z} \right] \quad (5)$$

where, ρ is the fluid density; μ is the kinematic viscosity; u, v, w are the component of velocity in Cartesian coordinates; p is the pressure term; F_x, F_y, F_z are the body force terms; T is temperature in Kelvins; Φ is the heat flux, C_p is the specific heat capacity, and k is the heat transfer coefficient. For numerical analysis, solution of governing equations is sought using control volume based numerical solver. Since the present study involves high Reynolds number turbulent flow, the N-S equations are numerically solved by Reynolds averaging also known as Reynolds-averaged Navier-Stokes (RANS). The RANS govern the transport of the averaged flow quantities, with the whole range of the scales of turbulence being modelled. For numerical analysis, Reynolds-averaged Navier-Stokes (RANS) set of equations are usually used to account for the time-dependent behaviour of flow (Moin 2010). RANS help in optimum utilization of computational resources by averaging the flow quantities over the entire range of turbulence scale (Anderson *et al.* 2016). RANS equations also cater for Reynolds stressors that form an important part of flow analysis. Double precision solver is used for high accuracy and fluid is taken as air with ideal gas properties. Density based solver is selected with explicit algorithm. 2nd order upwind scheme is selected in flow discretization and 1st order upwind scheme is used to cater for turbulent viscosity. Suitable relaxation parameters are applied to maintain a courant number of less than 1 (Masud *et al.* 2017; Arif *et al.* 2018a).

All surfaces of the aircraft are selected as no-slip walls. The domain is selected as pressure far field with suitable inputs for sea-level ground conditions for a low flight speed of $M = 0.2$ during the landing phase. The bottom surface is modelled as ground and selected as no-slip wall. The aircraft is incorporated with intake duct and exhaust nozzle for higher accuracy. It is important to note that the complexity of numerical analysis significantly increases due to the presence of both internal and external flows, however, the effect of intake and exhaust plays a significant role in aircraft stability characteristics, especially during the landing phase, and therefore included in this study. Evaluation of boundary conditions for intake duct and exhaust nozzle is a

complex task as it requires a complete analysis of the propulsion system. For this purpose, an analytical engine model already developed by the author (Arif *et al.* 2019) is utilized to ascertain the boundary conditions for intake and exhaust during the landing phase. The pressure and temperature boundary conditions at the intake duct and exhaust nozzle are evaluated for designed mass flow rate (*MFR*) conditions using the same analytical model.

3.4 Grid Generation and Independence Study

Grid generation is one of the key steps in numerical simulation. It is imperative to design and implement a smart grid scheme which is dense and fine enough to capture all flow phenomena accurately. However, this aspect needs to be balanced with available computational resources and time. For this study, we have employed a hybrid mesh scheme where the aircraft and HT geometries are meshed separately by unstructured mesh elements using elliptical refinement to maintain grid orthogonality at the aircraft surfaces and improve solution accuracy in near-wall region as shown in Fig. 2(a). Special emphasis has been laid to ensure that the sharp curves and important features such as wings, horizontal tails and landing gears are meshed with fine refined mesh. For these surfaces, a bottom-top approach is employed where the edge sizing is applied and subsequently face sizing is applied to control the mesh elements accordingly. A minimum mesh element size in streamwise coordinate $\Delta x = 1.12 \times 10^{-4}$ is set near the aircraft surfaces, whereas in the vertical direction the minimum mesh element size is set to $\Delta y = 5.3 \times 10^{-5}$ is set. The grid size is gradually increased away from the aircraft surface utilizing the inflation features for optimal computational requirements. A multi-layer prism is also applied on aircraft boundary to accurately capture boundary layer and near-wall effects (as shown in Fig. 2(b)). A total of 20 prism layers are applied on the aircraft fuselage, wings and tails to analyze the boundary layer characteristics and its associated unsteadiness precisely. The layers are inflated with a ratio of 1.001 until twice the size of local boundary layer thickness δ^* . Turbulent y^+ values are kept at an optimum level of less than 1 at aircraft surfaces for all flow conditions. Prime importance is given to maintain mesh consistency at all simulating conditions. Three different meshes are generated, namely, G1 (14.5 million), G2 (17.1 million) and G3 (19.8 million), based on the number of cells. Grid G2 is generated by refining the near-wall grid parameters of G1 by a factor of 0.8, whereas G3 is generated by further refining the near-wall grid size of G2 by a factor of 0.85. In order to select an optimum mesh size, a grid independence study is carried out before the final selection of mesh. For the said purpose, aerodynamic coefficient of lift at varying AoA at $M = 0.2$ without any HT deflection is calculated for all three grids and shown in Fig. 3(a). It is observed that the lift coefficients (C_l) are similar at low AoA ($0-4^\circ$) for all grids, however, at higher $AoAs$, a significant deviation of 12% in C_L for G1 is observed, whereas the C_L for G2 and G3 are almost similar. Hence, grid G2 is selected for further

analysis based on the balance between accuracy and the required computational resources.

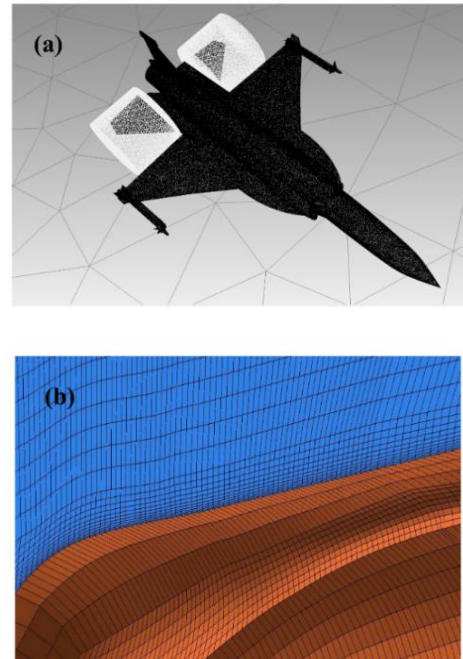


Fig. 2. (a) Meshed aircraft geometry with horizontal tails meshed in separate cylindrical domain and (b) prism layers over the aircraft fuselage surface.

The selection of turbulence model is as important as selection of grid size for numerical analysis, hence, this aspect cannot be ignored. For this research, three different models (SA, SST $k-\omega$ and $k-\epsilon$) are analyzed based on grid G2 keeping in view the complex flow phenomenon involving both internal flow (inside intake duct and exhaust nozzle) and external flow over the aircraft. SA is a single equation turbulence model while $k-\epsilon$ and SST $k-\omega$ are two-equation turbulence models (Kuntz and Menter 2004; Bulat and Bulat 2013). Comparative results of C_L for these models are presented in Fig. 3(b). Based on the results, it is observed that the variation of C_L obtained from S-A model and $k-\omega$ model is almost negligible, however, the results obtained from $k-\epsilon$ are under-predicted by an average of 21%. Also, the convergence stability and residuals from S-A and $k-\epsilon$ are not satisfactory as disordered sinusoidal behavior was observed throughout the simulations. Hence, $k-\omega$ turbulence model is selected for this research since it is a two-equation turbulence model that includes extra transport equations to evaluate turbulent properties of the fluid. The results are consistent and in agreement with previous research (Masud *et al.* 2017; Arif *et al.* 2018b).

3.5 Validation of Numerical Methods

The validation of complete numerical scheme is carried out with previous numerical study on similar aircraft (Masud *et al.* 2015) and OEM Wind Tunnel Data. The analysis is carried out at $M=0.2$ at varying AoA with grid G2 and SST $k-\omega$ model. The results

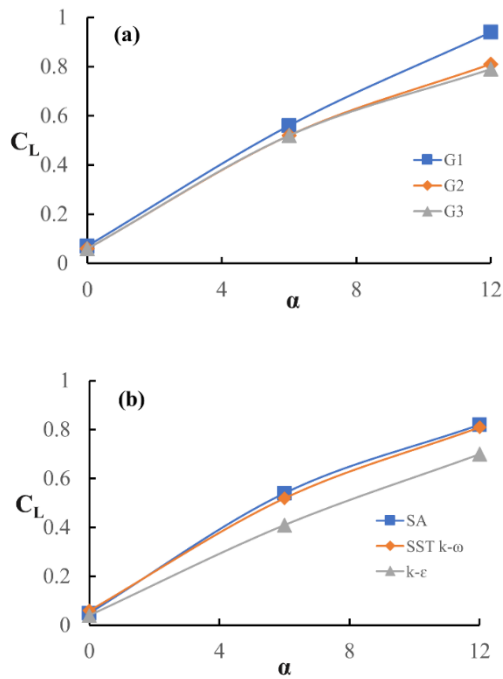


Fig. 3. (a) Grid independence and (b) turbulence model independence.

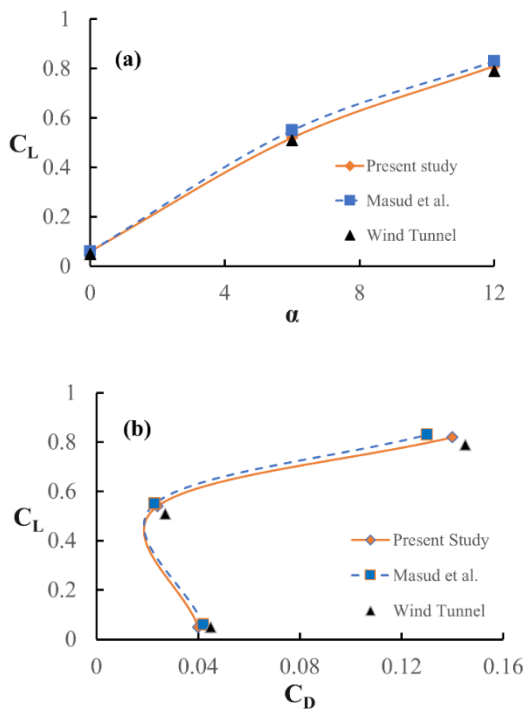


Fig. 4. Validation of numerical method. (a) Coefficient of lift and (b) drag polar.

for C_L and C_D (drag polar) evaluated from the present study, Masud *et al.* (Masud *et al.* 2015) and Wind Tunnel Data are shown in Fig. 4. An excellent agreement between the results is observed for our numerical scheme with Wind Tunnel Data for C_L . A slight deviation of 3.4% in C_D (drag polar) is observed in between the numerical results and Wind Tunnel Data which is attributed to the rise in drag

due to secondary landing gears doors in Wind Tunnel Model. Hence, from the verifications shown above, the numerical methods, grid size, and turbulence model are appropriate for the numerical simulations in the present research.

4. RESULTS AND DISCUSSIONS

The present study aims to evaluate the stability characteristics of the aircraft in an emergency situation of a single horizontal tail failure during flight due to which the aircraft is required to land immediately in the nearest airfield. For this situation, we aim to analyze the countermeasures (by operations of rudder, ailerons and a functional HT) during the landing. During the landing approach, the aircraft speed limit is restricted to Mach number of 0.2 and its maximum allowable AoA is 12° , as depicted in OEM flight manual. Furthermore, the range of HT, rudder and aileron deflections in this study are also considered according to the landing limits described in the flight manual. Hence, we have analyzed the stability characteristics of the aircraft in the present study keeping in view its landing limitations. The analysis is divided into 2 major parts. In the first part, aircraft stability characteristics at different flow conditions and different ground clearances in a single HT locked configuration is evaluated in detail. Later, the countermeasures for aircraft control and safe landing are evaluated by utilizing the available Wind Tunnel Data for control surfaces deflections. The analysis is carried out at five different right HT deflections (-5° , -6° , -8° , -10° , -15°) ranging from -5° to -15° and two different clearance heights from the ground (1m and 5m). For each condition, different asymmetric HT deflections are simulated where the left HT is kept at neutral position (failure state) and the right HT is deflected to different incidence angles. The simulations are progressed for a sufficient time until the solution shows statistically time-independent periodic behavior. All the calculated variables are based on time-averaged values which are evaluated once the solution is statistically stable. Due to the sensitivity and confidentiality of data, the magnitude of all moment coefficients has been normalized with respect to their relative maxima. The sign convention for aircraft stability characteristics and control surfaces generally differs in literature and may hinder the understanding of readers. Hence, it is important to set the sign convention of control surface deflections and aircraft stability coefficients at this instance for brevity. The left HT is considered locked to a neutral position of 0° due to its fail-safe characteristics, whereas the right HT is deflected with its leading-edge rotating downward and indicated by a negative deflection. The negative rolling moment coefficient in this study indicates the aircraft roll movement towards the right, whereas the negative yawing moment indicates the aircraft yaw towards the right direction.

4.1 Aerodynamics and Stability Characteristics with Variation of HT Deflection

The analysis is carried out with left HT locked in neutral position due to its failure and the right HT

is deflected at different incidence angles to study the aerodynamic behavior of aircraft. The coefficient of lift, drag polar, pitching moment, rolling moment and yawing moment experienced by the aircraft is evaluated and discussed in this section.

The coefficient of lift and drag polar for different right HT deflections at 1m ground clearance is plotted in Fig. 5. It is observed that the lift curve slope is constant for all HT deflections, however, the aircraft experiences a reduction in lift coefficient with an increase in HT deflection (Fig. 5(a)). A similar trend is observed for drag polar at different HT deflections where the drag polar shifts towards the right side with an increase in HT deflection. It is evident that the aircraft experiences an increase in drag with high HT deflection (Fig. 5(b)). Hence, it is important to monitor aircraft drag at each instance in order to effectively control the aircraft without any significant drag penalty.

The aircraft pitching moment (C_m) is considered with respect to aircraft centre of gravity (CG) which depends on major components such as wings, fuselage and control surfaces. The aircraft pitching moment, rolling moment and yawing moment are evaluated by (Williams and Vukelich 1979; Nelson 1998):

$$C_{m_{cg}} = C_{m_{0_w}} + C_{L_w} \left(\frac{x_{cg}}{c} - \frac{x_{ac}}{c} \right) - \eta \frac{S_t}{S} C_{L_t} \left[\frac{l_t}{c} - \left(\frac{x_{cg}}{c} - \frac{x_{ac}}{c} \right) \right] + C_{m_f} + C_{m_{0_t}} \quad (6)$$

$$C_{l_\beta} = (C_{l_\beta})_{WB} + \sum_p \left\{ (C_{Y_\beta})_p \left[\frac{z_p \cos \alpha - l_p \sin \alpha}{b_w} \right] \right\} \quad (7)$$

$$C_{n_\beta} = (C_{n_\beta})_{WB} + \sum_p -(\Delta C_{Y_\beta})_p \left(\frac{l_p + (x_{a.c})_p}{b_w} \right) \quad (8)$$

where, $\eta = Q_t/Q$ is the tail efficiency factor; $V_H = l_t S_t / c S$ is the tail volume parameter; $(C_{l_\beta})_{WB}$ represents the contribution of wing-body configuration; $(\Delta C_{Y_\beta})_p$ is the side force due to the sideslip of the added vertical surfaces; $(C_{n_\beta})_{WB}$ is the contribution from wing-body combination to the total yawing moment due to slip; $(\Delta C_{Y_\beta})_p$ is the added force due to the side-slip of vertical surfaces; z_p is the normal distance between the moment center and aerodynamic center of vertical panel; l_p is the distance between vehicle moment center and the quarter-chord; b_w is the span of the wing; $(x_{a.c})_p$ is the distance parallel to the longitudinal axis between the quarter-chord and the aerodynamic center of vertical surface.

Aircraft stability coefficients with different HT deflections at 1m ground clearance is shown in Fig. 6. From Fig. 6(a), it is evident that the right HT deflection assists in aircraft longitudinal stability as the slope of curve is found to be negative. However, it is important to identify the trim AoA for the aircraft

for its safe control with respect to its pitching motion. The aircraft under study has a maximum limit of 12° for safe landing, hence the HT deflection must allow the aircraft to land within this AoA limit. It is observed that the trim AoA for a HT deflection of -5° is observed to be 8.5° , whereas the trim AoA increases with an increase in HT deflection. For a HT deflection of 15° , the trim AoA exceeds our analysis results and data is extrapolated to identify the trim condition. The results at each HT deflection are summarized in Table 1.

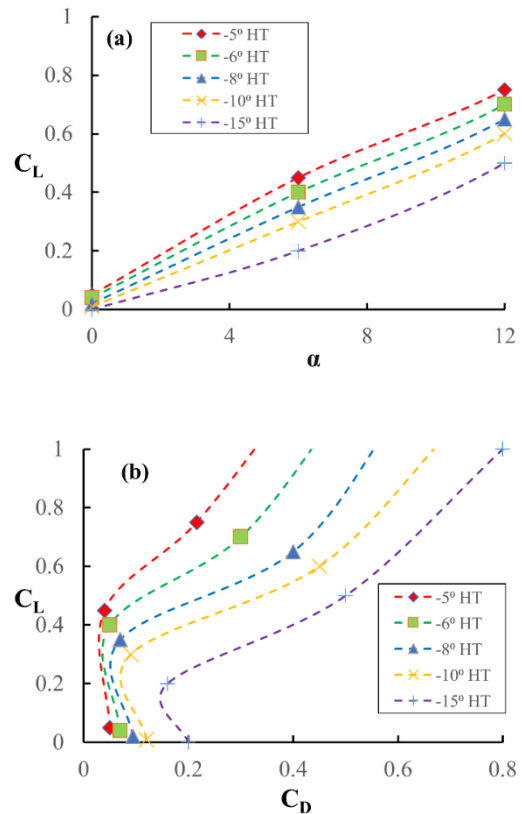


Fig. 5. (a) Coefficient of lift and (b) drag polar.

Rolling moment experienced by the aircraft is shown in Fig. 6(b). It is observed that the rolling moment coefficient decreases with an increase in HT deflection. The aircraft experience a negative rolling moment in each case and would require certain aileron deflection to counter the adverse rolling moment which would be evaluated in the subsequent section. The yawing moment experienced by the aircraft with different HT deflections is also shown in Fig. 6(c). No significant change in yawing moment coefficient is observed with an increase in AoA, however, the yawing moment significantly decreases with an increase in HT deflection. To counter the adverse yawing moments experienced by the aircraft, certain rudder deflections would be required which are ascertained in subsequent sections.

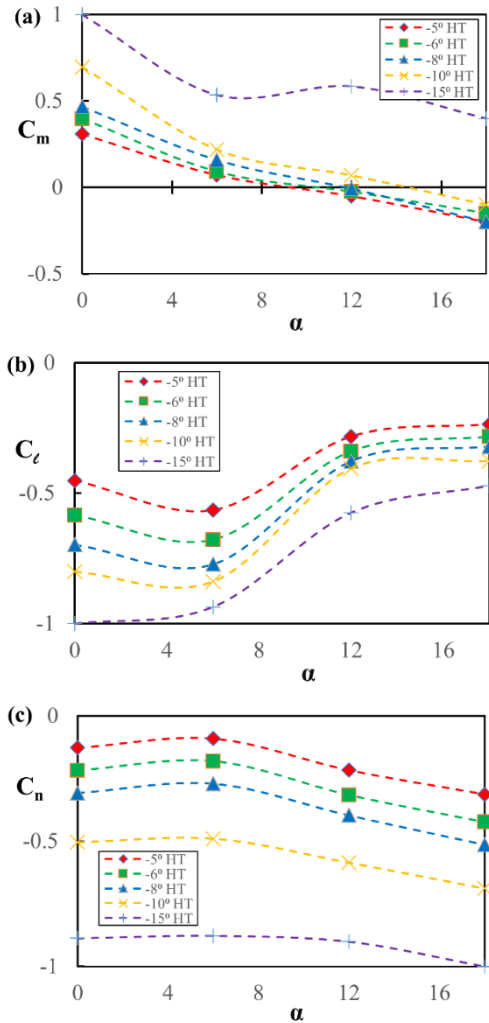


Fig. 6. Coefficient of (a) pitching moment, (b) rolling moment and (c) yawing moment.

Table 1 Trim AoA for different HT deflections

HT Deflection	Ground Clearance	Trim AoA
-5	1 m	~ 8.5°
	5 m	~ 7.5°
-6	1 m	~ 9.5°
	5 m	~ 9°
-8	1 m	~ 12°
	5 m	~ 10.7°
-10	1 m	~ 14.5°
	5 m	~ 13.2°
-15	1 m	~ 25°
	5 m	~ 23°

4.2 Aerodynamics and Stability Characteristics with Variation of Height

To analyze the aircraft aerodynamic characteristics at different ground clearance height, the lift, drag,

and stability coefficients are evaluated at two different ground clearances, i.e. 1m and 5m height for HT deflection of -5° . Fig. 7 shows the lift and drag coefficients of aircraft with variation of height. It is observed that the lift coefficient is reduced by an average of $\sim 9.6\%$ at lower ground clearance. The reduction in aircraft lift is attributed to strong wingtip vortices in the vicinity of ground which results in a downwash component on aircraft wing. A rise in drag by $\sim 19\%$ is also evident in drag polar plot at different heights where a relatively lower drag is experienced by the aircraft at high ground clearance as compared to low ground clearance. The fact is attributed to the drag penalty induced by landing gears at low ground clearance which significantly affects the overall aircraft behavior during landing. Hence it indicates that the aircraft would require certain changes in control surfaces deflections while approaching near the ground in this emergency situation.

The pitching moment coefficient illustrated in Fig. 8(a) also shows a significant change in the aircraft longitudinal stability with different ground clearance height, where a lower trim AoA of 7.5° is required at high ground level as compared to 8.5° for low ground level. The requirement of trim AoA is increased at lower ground level to safely land the aircraft. However, no significant change in rolling and yawing moment coefficients are observed as shown in Fig. 8(b) and (c).

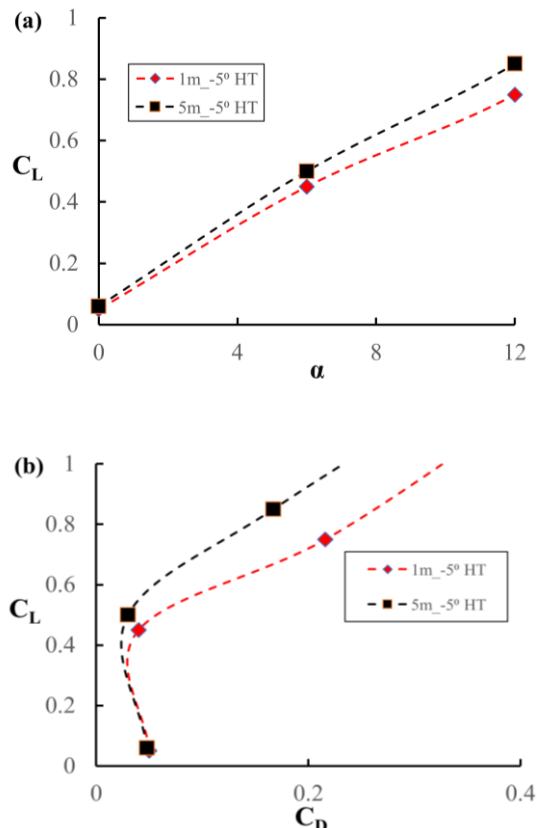


Fig. 7. (a) Lift and (b) drag variation with ground clearance.

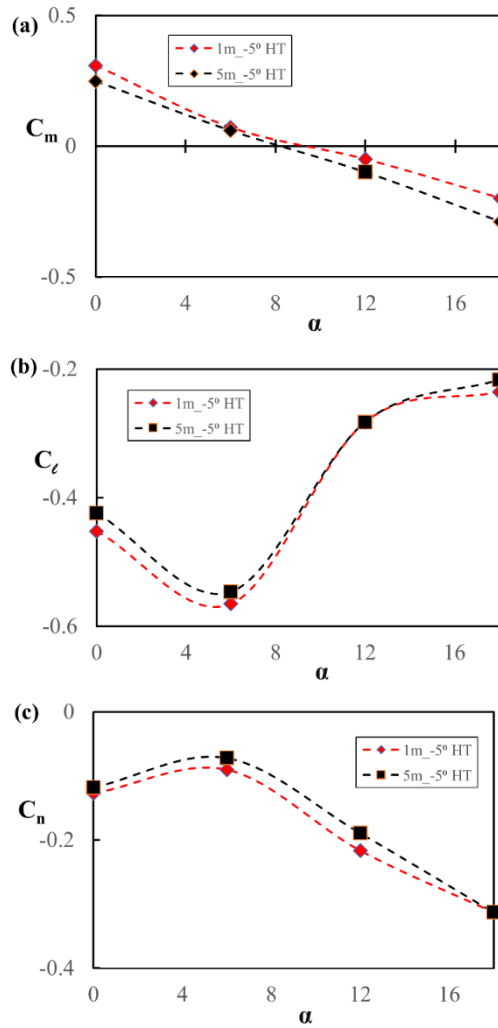


Fig. 8. (a) Pitching, (b) rolling and (c) yawing moment variation with ground clearance.

4.3 Flow Field Analysis

To investigate the aircraft characteristics at different ground clearances and the effect of ground on aircraft stability, pressure field plots and streamlines are plotted and shown in Fig. 9 at $AoA = 12^\circ$. The left HT is locked at neutral position whereas the right HT is deflected at -5° . For brevity, the pressure contour plots are shown for half domain only to clearly visualize the effect of ground during landing. Figure 9(a) shows the static pressure field around the aircraft just before landing at a ground clearance of 1m. The effect of low ground clearance is clearly observed underneath the fuselage and around the exhaust where its plume is significantly deflected due to ground. The Mach discs formed within exhaust plume experience a sudden disruption due to ground and subsequently generates a stagnation region of high pressure underneath the aircraft rear fuselage area. As a consequence, the aircraft experiences additional pitching moment which results in an increase in trim AoA as observed in Fig. 8(a). On the other hand, the aircraft at 5m ground clearance in Fig. 9(b) does not experience any significant deviation in pressure field around the aircraft and exhaust plume which is also observed in Fig. 7 and Fig. 8. To

further investigate the flow behavior around the aircraft during landing, the streamlines of total pressure over the aircraft are plotted at 1m and 5m ground clearance at $AoA = 12^\circ$ in Fig. 9(c) and Fig. 9(d) respectively. Note that the landing gears are hidden in the plot for a clear view. The streamlines at 5m height beneath the aircraft in fuselage and wing areas are quite smooth and no disruption is observed. However, at low ground clearance, a significant flow distortion underneath the aircraft can be observed. The flow tends to deviate away from the aircraft in spanwise direction and also results in strong wingtip vortices. This effect also results in a strong downwash component on the aircraft wing as results in lower lift as observed in Fig 8. Furthermore, severe distortion in flow is also observed in a landing gear bay due to high induced drag. Hence, it can be easily ascertained that the stability characteristics of aircraft are significantly affected in the present situation during landing. Therefore, we would evaluate the safe flight envelope for safe aircraft landing with a single HT locked situation in subsequent sections.

4.4 Counter Measures for Aircraft Control

4.4.1 Control Surfaces Effectiveness

In this section, the countermeasures required to control the aircraft with control surfaces deflection for safe landing with left HT locked position is evaluated. Wind tunnel data which has already been validated in prior studies (Masud *et al.* 2017) is utilized to evaluate the required control surfaces deflections. The available data provides the HT effectiveness for asymmetric deflections where both the HT are deflected. We, therefore, re-evaluated the wind tunnel data of control surfaces data for the current condition of left HT locked (0°) and right HT deflected to reflect the same asymmetry condition.

Figure 10(a) shows the rolling moment coefficient based on different aileron deflections. It is observed that the magnitude of rolling moment coefficient increases with higher aileron deflection. The slope of change in rolling moment is almost constant for each deflection, however, the higher deflection would allow the aircraft to counter the adverse rolling moments much effectively. The yawing moments for different rudder deflections are shown in Fig. 10(b). The magnitude of the rudder effectiveness increases with higher rudder deflections whereas the overall slope is similar for each rudder deflection.

4.4.2 Estimation of Counter Measures

In this section, the control deflections required to counter the adverse moments encountered by the aircraft are evaluated for safe landing keeping in view the aircraft maneuverability limitations. Two different schemes can be adopted to determine the safe landings. Firstly, the differential between aircraft moment coefficients and control surface effectiveness can be evaluated to determine the control point where the plot intersects y-axis. Secondly, the magnitude of aircraft moment coefficients and control surface effectiveness can be plotted and the control point can be determined

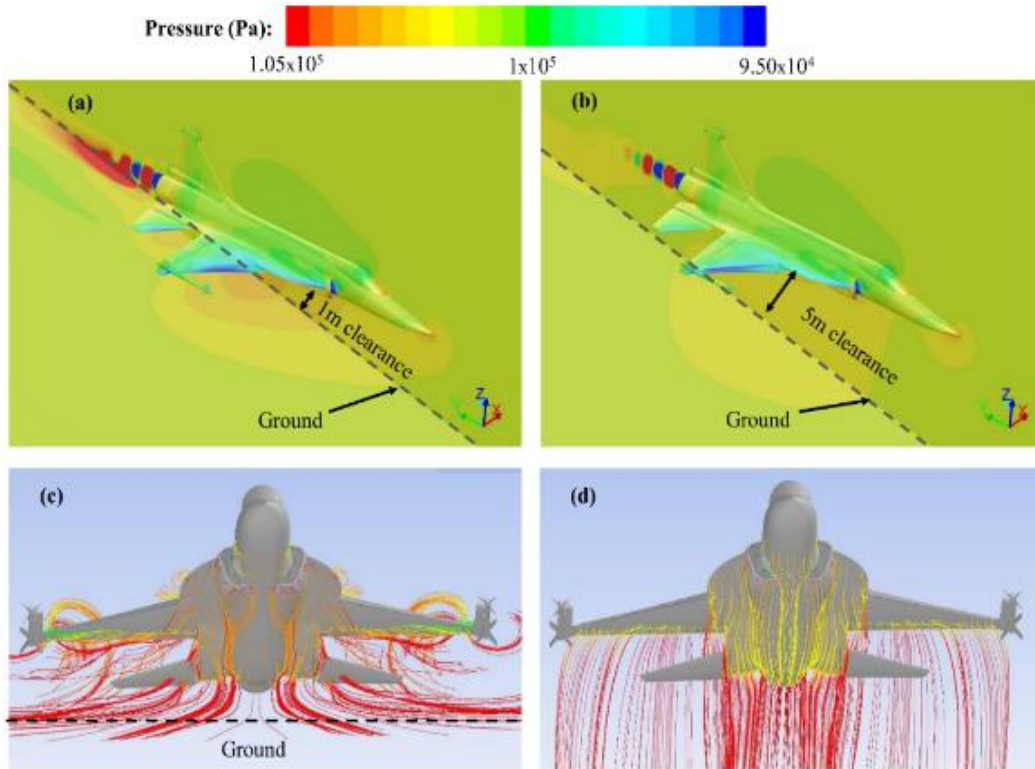


Fig. 9. (a) Pressure field at 1m ground clearance, (b) pressure field at 5m ground clearance, (c) pressure streamlines at 1m ground clearance and (d) pressure streamlines at 5m ground clearance. All figures are shown at $AoA = 12^\circ$ (landing gears hidden for clarity).

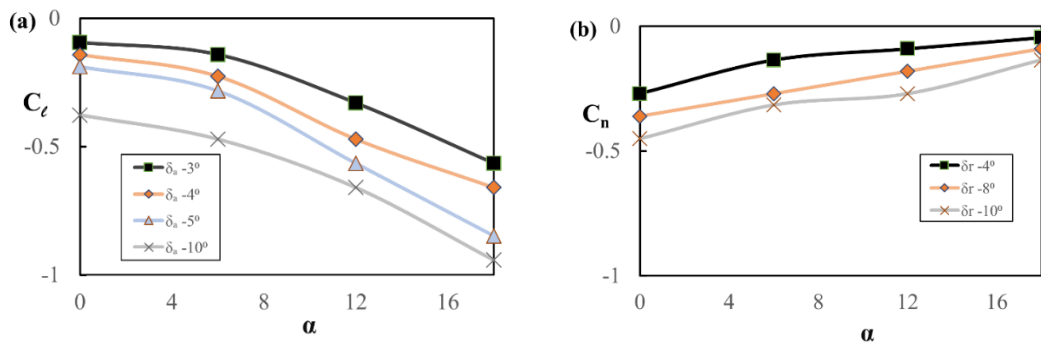


Fig. 10. Control surfaces effectiveness.

where the two lines intersect each other. Since we are interested in determining the complete envelope of safe landing rather than distinct conditions, we adopted the second scheme where the magnitudes of coefficient are plotted and intersection points are analyzed. Fig. 11 shows the aircraft roll moment coefficients along with aileron effectiveness. It is important to note that the maximum allowable landing AoA for the aircraft is 12° whereas the minimum AoA is 7° . From the plot, the aileron control deflection to counter the adverse rolling moment can be ascertained at all flight conditions included in this study. The maximum and minimum allowable landing AoA are marked as red vertical lines in the plot whereas the complete allowable envelope is indicated by shaded area on the plot. As an example, it can be observed that the aileron

deflection of 10° can counter the adverse rolling moment of aircraft at $\sim 7.1^\circ$ AoA for -5° HT deflection, $\sim 8.5^\circ$ for -6° HT deflection, $\sim 9.2^\circ$ for -8° HT deflection, $\sim 9.6^\circ$ for -10° HT deflection and $\sim 11^\circ$ for -15° HT deflection.

Similarly, the rudder deflections required to control the aircraft are evaluated and shown in Fig. 12. The complete allowable envelope is indicated by shaded area on the plot. It is observed that a rudder deflection of 10° can counter the adverse yawing moment of aircraft at $\sim 13^\circ$ AoA for -5° HT deflection (not within safe limit), $\sim 10.5^\circ$ AoA for -6° HT deflection and $\sim 7^\circ$ AoA for -8° HT deflection, whereas for -10° and -15° HT deflections, the rudder deflections of $\leq 10^\circ$ are not able to counter the adverse yawing moment. Hence, the determination

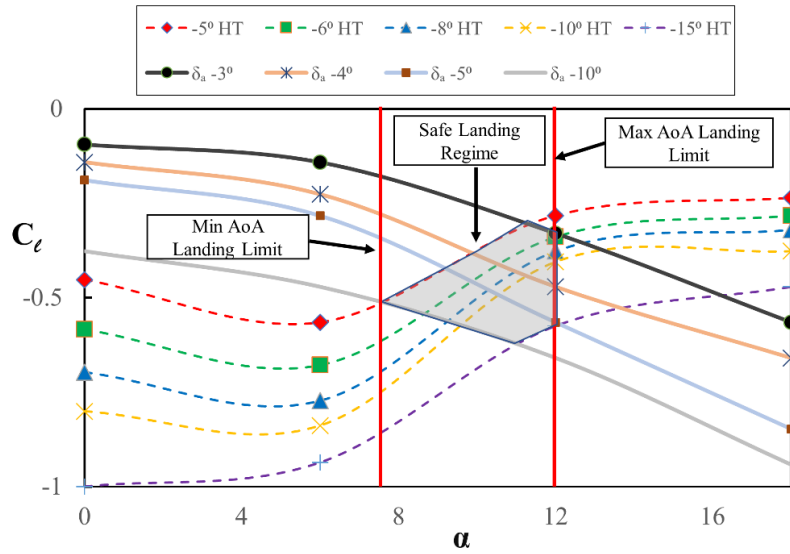


Fig. 11. Evaluation of countermeasures for rolling moment at 1m ground clearance.

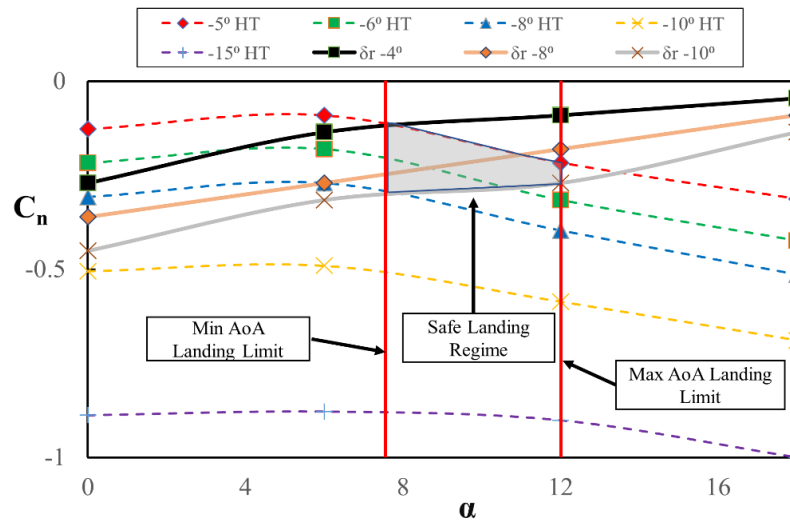


Fig. 12. Evaluation of countermeasures for yawing moment at 1m ground clearance.

of countermeasures for safe landing requires careful evaluation of both aileron and rudder deflections while maintain an allowable AoA . To analyze the safe limits for each HT deflection, a summary of the required control surfaces deflection against different landing AoA is presented in Table 2.

A complete safe landing envelope can be evaluated in case of a left HT failure where it locks to neutral position (0°), the right HT can be deflected up to a maximum of 8° since the maximum landing AoA limit for the aircraft is 12° . For 5° deflection of functional HT, a minimum aileron deflection of 7° and a minimum rudder deflection of 5° is required for safe landing, whereas for 8° deflection of HT, a minimum aileron deflection of 3° and a minimum rudder deflection of 14° is required.

Table 2 Required control surfaces deflections for safe landing

Right HT Deflection	Landing AoA	Required Aileron Deflection	Required Rudder Deflection
-5°	$\sim 8.5^\circ$	$\sim 7^\circ$	$\sim 5^\circ$
-6°	$\sim 9.5^\circ$	$\sim 6^\circ$	$\sim 6^\circ$
-8°	$\sim 12^\circ$	$\sim 3^\circ$	$\sim 14^\circ$
-10°	$\sim 14.5^\circ$	$\sim 2^\circ$	Not possible
-15°	$\sim 25^\circ$	Not possible	Not possible

5. CONCLUSIONS

In this study, numerical analysis of an aircraft in a possible emergency situation of a single horizontal tail (HT) failure is carried out to analyze its stability characteristics and evaluate the countermeasures for its safe landing. A comprehensive solution strategy is designed and employed where the HTs are embedded in separate cylindrical domains to facilitate their movements without disrupting the aircraft domain and hence maintaining high accuracy of numerical results and saving 60% of the computational time. The numerical methodology is validated with the literature and Wind Tunnel Data and an excellent agreement is observed. Subsequently, analysis of aircraft at different flow conditions and different ground clearances in a single HT locked configuration (left HT locked in neutral position) is evaluated in detail. The analysis is carried out at five different right HT deflections (-5° , -6° , -8° , -10° , -15°) ranging from -5° to -15° and two different clearance heights from the ground (1m and 5m). For each condition, different asymmetric HT deflections are simulated where the left HT is kept at neutral position (failure state) and the right HT is deflected to different incidence angles.

Analysis reveals that the right HT deflection results in a decrease in lift and high HT deflections require high trim $A\alpha$ to maintain the longitudinal stability of aircraft. The rolling moment coefficient decreases with an increase in HT deflection, however, the yawing moment significantly decreases with an increase in HT deflection. Analysis at different ground clearance heights reveals that the lift coefficient is reduced by an average of $\sim 9.6\%$ at lower ground clearance which is attributed to strong wingtip vortices in the vicinity of ground. A rise in drag by $\sim 19\%$ is also observed lower ground clearance due to the drag penalty induced by landing gears at low ground clearance which significantly affects the overall aircraft behavior during landing.

The control deflections required to counter the adverse moments encountered by the aircraft are also evaluated for safe landing keeping in view the aircraft maneuverability limitations. A complete flight envelope for safe landing is developed based on right HT, ailerons and rudder deflections. The study can help in further improvement of the aircraft flight control computer to restrict the tail, aileron and rudder deflections up to the evaluated safe limits. Also, the designed methodology applies to all similar aircraft.

ACKNOWLEDGMENTS

The authors acknowledge the use of Numerical Analysis Lab (NAL) of College of Aeronautical Engineering, Risalpur, Pakistan for numerical simulations.

REFERENCES

Anderson, D., J. C. Tannehill and R. H. Pletcher (2016). *Computational fluid mechanics and*

heat transfer, Taylor & Francis.

Arif, I., J. Masud and I. Shah (2018a). Computational Analysis of Integrated Engine Exhaust Nozzle on a Supersonic Fighter Aircraft. *Journal of Applied Fluid Mechanics* 11(6), 1511-1520.

Arif, I., J. Masud, A. Javed, Z. G. Toor and S. H. R. Shah (2019). Analytical Modelling and Validation of a Turbofan Engine at Design Conditions. *AIAA Scitech* 2019 Forum.

Arif, I., S. Salamat, M. Ahmed, F. Qureshi and S. Irtiza Ali Shah (2018b). Comparative Flow Field Analysis of Boundary Layer Diverter Intake and Diverterless Supersonic Intake Configuration. *Journal of Applied Fluid Mechanics* 11(4), 1125-1131.

Bulat, M. P. and P. V. Bulat (2013). Comparison of turbulence models in the calculation of supersonic separated flows. *World Applied Sciences Journal* 27(10), 1263-1266.

Chyu, W. and L. Schiff (1983). Nonlinear aerodynamic modeling of flap oscillations in transonic flow-A numerical validation. *AIAA Journal* 21(1), 106-113.

Cook, M. V. (2012). *Flight dynamics principles: a linear systems approach to aircraft stability and control*, Butterworth-Heinemann.

Green, L., A. Spence and P. Murphy (2004). Computational methods for dynamic stability and control derivatives. *42nd AIAA Aerospace Sciences Meeting and Exhibit*. USA. AIAA 2004-15

Hua, Y., S. Lei and C. Weifang (2017). Research on parafoil stability using a rapid estimate model. *Chinese Journal of Aeronautics* 30(5), 1670-1680.

Hui, W. and M. Tobak (1984). Bifurcation analysis of aircraft pitching motions about large mean angles of attack. *Journal of Guidance, Control, and Dynamics* 7(1), 113-122.

Jing, W., W. Yankui and D. Xueying (2016). An experimental investigation on static directional stability. *Chinese Journal of Aeronautics* 29(6), 1527-1540.

Kimberlin, R. D. (2003). *Flight testing of fixed-wing aircraft*, American Institute of Aeronautics and Astronautics.

Kuntz, M. and F. Menter (2004). Simulation of fluid-structure interactions in aeronautical applications. *European Congress on Computational Methods in Applied Sciences and Engineering*, Eccomas Jyväskylä, Finland.

Masud, J. and F. Akram (2011). Flow field and performance analysis of an integrated diverterless supersonic inlet. *Aeronautical Journal* 115(1170): 471.

Masud, J., I. Arif and Z. Toor (2017). Composite Analysis and Characterization of Exhaust Effects on Aerodynamic Behavior of a

- Supersonic Aircraft. *55th AIAA Aerospace Sciences Meeting*. USA. AIAA 2017-0269.
- Masud, J., O. Khan and S. M. Hassan (2015). Intake and Airframe Characterization through Composite CFD. *53rd AIAA Aerospace Sciences Meeting*. USA. AIAA 2015-1669.
- Moin, P. (2010). *Fundamentals of engineering numerical analysis*, Cambridge University Press.
- Murman, S., S. Pandya and N. Chaderjian (2002). Automation of a Navier-Stokes S&C database generation for the Harrier in Ground Effect. *40th AIAA Aerospace Sciences Meeting & Exhibit*. USA. AIAA 2002-0259
- Neal, D., M. Good, C. Johnston, H. Robertshaw, W. Mason and D. Inman (2004). Design and wind-tunnel analysis of a fully adaptive aircraft configuration. *45th AIAA/ASME/ASCE/AHS/ASC Structures, Structural Dynamics & Materials Conference*. USA. AIAA 2004-1727
- Nelson, R. C. (1998). *Flight stability and automatic control*, WCB/McGraw Hill New York.
- Orlik-Rückemann, K. J. (1975). Dynamic stability testing of aircraft—needs versus capabilities. *Progress in Aerospace Sciences* 16(4), 431-447.
- Park, M., L. Green, R. Montgomery and D. Raney (1999). Determination of stability and control derivatives using computational fluid dynamics and automatic differentiation. 17th Applied Aerodynamics Conference. USA. AIAA 99-3136
- Raymer, D. (2012). *Aircraft design: a conceptual approach*, American Institute of Aeronautics and Astronautics, Inc.
- Regan, C. (2008). In-flight stability analysis of the X-48B aircraft. *AIAA atmospheric flight mechanics conference and exhibit*. USA. AIAA 2008-6571
- Rogers, S., M. Aftosmis, S. Pandya, N. Chaderjian, E. Tejnil and J. Ahmad (2003). Automated CFD parameter studies on distributed parallel computers. *16th AIAA Computational Fluid Dynamics Conference*. USA. AIAA 2003-4229
- Stevens, B. L., F. L. Lewis and E. N. Johnson (2015). *Aircraft control and simulation: dynamics, controls design, and autonomous systems*, John Wiley & Sons.
- Williams, J. E. and S. R. Vukelich (1979). *The USAF stability and control digital DATCOM*. Volume I. Users manual, McDonnell Douglas Astronautics Co St Louis Mo.
- Zhiquan, L. and X. Pinqi (2017). Aeroelastic stability of full-span tiltrotor aircraft model in forward flight. *Chinese Journal of Aeronautics* 30(6), 1885-1894.